Journal of
Synchrotron Radiation

ISSN 1600-5775

Received 29 September 2014
Accepted 26 November 2014

Thermal stress prediction in mirror and multilayer coatings

Xianchao Cheng,* Lin Zhang, Christian Morawe and Manuel Sanchez del Rio

European Synchrotron Radiation Facility, 71 avenue des Martyrs, 38000 Grenoble, France.
*E-mail: chengxc@mail.ustc.edu.cn

Multilayer optics for X-rays typically consist of hundreds of periods of two types of alternating sub-layers which are coated on a silicon substrate. The thickness of the coating is well below 1 μm (tens or hundreds of nanometers). The high aspect ratio ($\sim 10^7$) between the size of the optics and the thickness of the multilayer can lead to a huge number of elements ($\sim 10^{16}$) for the numerical simulation (by finite-element analysis using *ANSYS* code). In this work, the finite-element model for thermal-structural analysis of multilayer optics has been implemented using the *ANSYS* layer-functioned elements. The number of meshed elements is considerably reduced and the number of sub-layers feasible for the present computers is increased significantly. Based on this technique, single-layer coated mirrors and multilayer monochromators cooled by water or liquid nitrogen are studied with typical parameters of heat-load, cooling and geometry. The effects of cooling-down of the optics and heating of the X-ray beam are described. It is shown that the influences from the coating on temperature and deformation are negligible. However, large stresses are induced in the layers due to the different thermal expansion coefficients between the layer and the substrate materials, which is the critical issue for the survival of the optics. This is particularly true for the liquid-nitrogen cooling condition. The material properties of thin multilayer films are applied in the simulation to predict the layer thermal stresses with more precision.

Keywords: multilayer optics; finite-element analysis (FEA); thermal mismatch; thermal stress; liquid-nitrogen cooling.

1. Introduction

During the last ten years, more than half of all ESRF (the European Synchrotron Radiation Facility) beamlines have been equipped with multilayer-based X-ray optics. One of the most demanded applications would be multilayer white-beam monochromators, which will play an important role in improving the beamline performances for the ESRF Upgrade Program (2009–2015). Potential damage due to the heat load from the light source is a critical issue for the design of multilayer-based white-beam optics. Previous experiments of both *in situ* irradiation study and *ex situ* X-ray reflectivity test have been conducted to investigate the degradation mechanisms for multilayer optics under synchrotron white-beam exposure (Friedrich *et al.*, 2011). It is indicated that the multilayer structure is heavily damaged when it is exposed in air and the reflectivity stays stable when it is exposed in nitrogen. The multilayer is most probably damaged by chemical reaction with oxygen induced by the photon effect or thermal effects.

High-heat-load-induced thermal deformation in X-ray optics has been investigated intensively in the synchrotron community. To minimize the thermal deformation, the routinely adopted methods at ESRF and many other light sources are: water cooling combined with smart-cut geometry for white-beam mirrors and some multilayer optics; liquid-nitrogen cooling for silicon crystal monochromators and some multilayer optics on silicon substrates. For typical multilayer optics, the thickness of the coatings is well below 1 μm (tens or hundreds of nanometers). Therefore, the influence of the coatings on the temperature distribution and thermal deformation of the substrate is generally negligible. Nevertheless, the thermal stress within the coated layers can be very significant due to different thermal expansion coefficients (CTEs) between the layer and substrate materials. This is particularly true for the liquid-nitrogen cooling condition. The thermal stress within the coatings has not been studied in detail due to the difficulties related to the very small thickness of the layers, such as (i) the high aspect ratio ($>10^6$) between the substrate size (~ 100 mm) and the coating thickness (~ 100 nm) for numerical simulation [by finite-element analysis (FEA)], (ii) very limited data on material properties of the thin layers which may be significantly different from bulk materials.

The layer thermal stress can be solved analytically for uniform temperature variation of the multilayer system (Hsueh, 2002). For synchrotron applications, the area illuminated by X-rays on the optics surface (footprint) is usually much smaller than the optics surface area. Therefore, a non-uniform temperature variation is induced. The temperature distribution is tri-dimensional, and depends on heat-load parameters, cooling conditions, material properties, and geometries of the substrate and the coating. For the multilayer X-ray optics, what is the stress and thermal deformation in the coated layers? Can the thin-film layers withstand the thermal stress induced by the heat load? What are the influences of the cooling conditions on the thermal stress and deformation? How can this thermal stress and deformation analysis guide the selection of the coating materials? This work contributes to answer these questions.

In this paper, the finite-element model for thermal-structural analysis of multilayer optics is implemented using the *ANSYS* layer-functioned elements. Single-layer coated mirrors and multilayer monochromators cooled by water or liquid nitrogen are studied with typical parameters. The material properties of thin multilayer films are applied to predict the layer thermal stresses with more precision.

2. Finite-element modeling of multilayer optics

Some special elements with layer functions are available in *ANSYS* which means that the properties of each sub-layer can be defined inside. One geometrical layer of elements contains multiple physically meaningful sub-layers which can have different properties, such as different materials and thicknesses. This one geometrical layer of elements allows a larger number of sub-layers with only one layer of finite elements to be described. Therefore the number of meshed elements is considerably reduced. According to various element properties, the types of elements used for thermal analysis and structural analysis are different. More detailed description about the elements can be found in the *ANSYS* documentation *Element Reference*.

For the model of multilayer optics, the type of element for thermal analysis is SHELL131. The number of sub-layers is limited to 31 maximum. For multilayer optics with more than 31 sub-layers, which are very common for practical applications, multi-shells are used and they are connected by constraint equations. The modeling process is shown in Fig. 1 with an example containing 40 sub-layers. Based on the substrate meshing (Fig. 1*a*), one shell of SHELL131 elements containing 20 sub-layers is generated from the top surface of the substrate (Fig. 1*b*). The same meshing as the top surface of the substrate is obtained in this way. Secondly, another shell containing 20 sub-layers is generated by copying the first shell with a positive offset. The generation is performed twice (Fig. 1*c*). The bottom shell on the top surface of the substrate is deleted after the generation. Thirdly, the nodes on the adjacent interfaces of the shells are connected using constraint equations (Fig. 1*c*). More precisely speaking, for nodes at the same X,Z position but in the two adjacent shells, the temperature on the top sub-layer in the lower shell is set to be equal to the temperature on the bottom sub-layer in the higher shell. The operation is repeated for all the nodes on each shell. The lowest shell is also connected to the substrate by this method.

The structural analysis model of the multilayer optics is reconstructed by using solid-type multilayer elements (SOLSH190). For the SOLSH190, the number of sub-layers is not limited and all the sub-layers are defined in one section. To apply the temperature loads from the result of the thermal analysis, the temperatures are stored in internal arrays after the thermal analysis. The difficulty is to find the correspondence between the elements in the thermal analysis model based on SHELL131 and those in the mechanical analysis model based on SOLSH190. As shown by the green dashed line in Fig. 2, the node numbers at the lowest (bottom) shell of the thermal model can correspond to the node numbers at the top surface of the structural model. For the two nodes at the same X,Z position, one at the lowest shell of the thermal model and the other at the top surface of the structural model, the node numbers are equal to each other. Based on this, the node numbers of the nodes at the lowest shell of the thermal

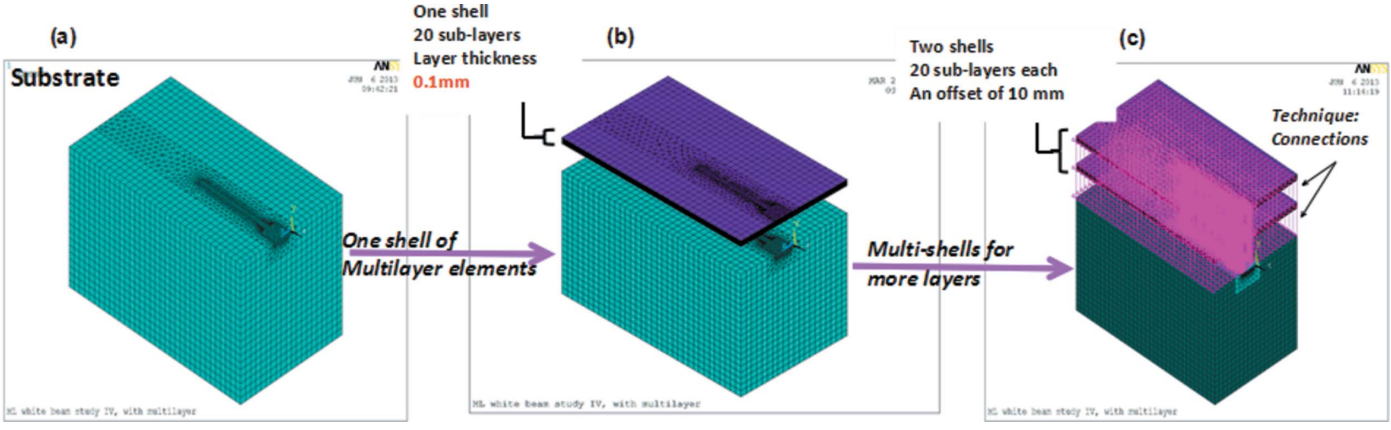

Figure 1
Modeling process for the multilayer thermal analysis model: substrate meshing (*a*); one shell generated (*b*); multi-shells and connections (*c*).

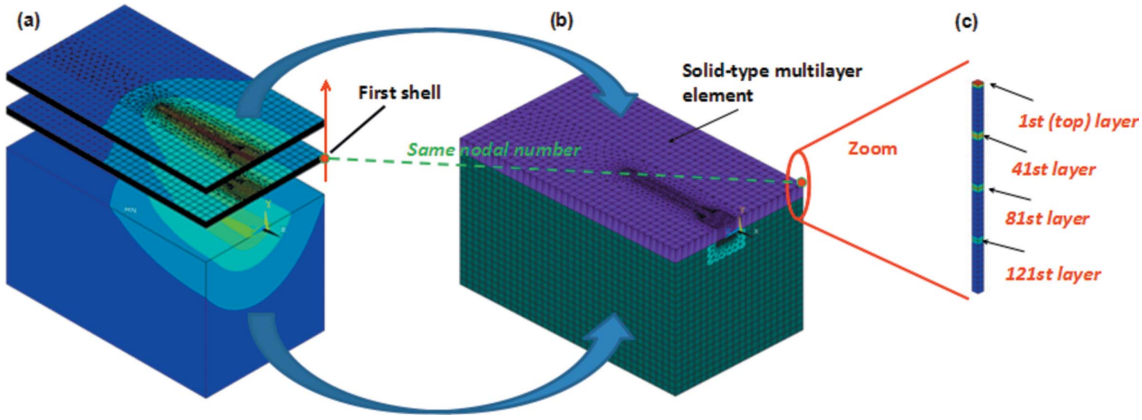

Figure 2
Graph for the temperature transfer process: temperature result of thermal analysis (*a*), structural analysis model reconstructed by SOLSH190 (*b*), schematic for applying temperature loads to individual sub-layer (*c*).

model are used to identify the X,Z position, which makes a bridge to the structural analysis model.

The thermal-structural coupled analysis model of multilayer optics has been implemented by using *ANSYS* layer-functioned elements. Both steady-state and transient analysis are able to be performed. Different material models, such as plasticity, hyper-elasticity, stress stiffening, creep, large deflection and large strain capabilities, are available for the layer-functioned elements. The multilayer model can be built based on the substrate meshing. The number of elements is reduced by a factor of 31 maximum for thermal analysis and by a factor of the number of sub-layers for structural analysis. The number of sub-layers feasible for the present computers is increased a lot. A model with more than 1000 sub-layers has been successfully tested.

3. Thermal stress prediction

In this section, single-layer coated mirrors and multilayer monochromators cooled by water or liquid nitrogen are studied by FEA with typical heat-load, cooling and geometrical parameters. The effects of cooling down of the optics and heating of the X-ray beam have been detailed. Initially, the material properties used for the simulation are the bulk values from the literature. In a second step, thin-film material properties are applied in the calculation.

3.1. Single-layer white-beam mirror

A test model with typical parameters of the white-beam mirror is shown in Fig. 3. A B_4C layer with a thickness of 50 nm is coated on silicon substrate of size 60 mm × 60 mm × 500 mm. The mirror is very long (500 mm) as the grazing angle for the total reflection of X-rays is very small. The upstream slits size is 4 mm × 2 mm (H × V). The power density from the light source is taken as P_a = 100 W mm^{-2}. With grazing angle α_{inc} = 5 mrad, the footprint length is 2 mm/sin(α_{inc}) = 400 mm, which does not overfill the surface. For the FEA, a quarter of the model is used with symmetry boundary conditions on two faces. As the red part in Fig. 3, uniform heat flux on the surface of the layer is applied. The cooling is applied on the side face.

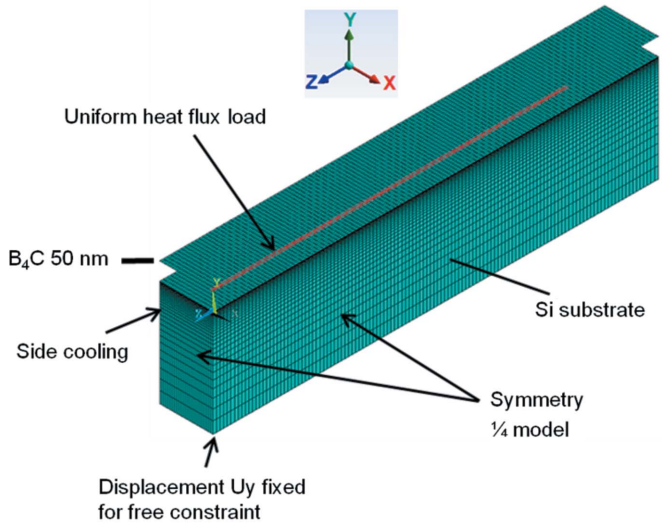

Figure 3
Single-layer mirror: FE model (for thermal analysis) and boundary conditions.

Water cooling and liquid-nitrogen cooling conditions are studied. The displacement along the vertical direction (U_y) is constrained at one point for the structural analysis.

3.1.1. Water cooling condition. The convection coefficient and cooling temperature are h_{cv} = 0.005 W mm^{-2} K^{-1} and T_{cool} = 293 K for the water cooling. Material properties of Si and B_4C are listed in Table 1.[1] The elastically anisotropic material properties of Si and others are not taken into account as only the layer in-plane direction is concerned for the simulation here.

The temperature distribution is plotted in Fig. 4(*a*). The maximum temperature (T_max) is calculated to be 313.8 K and the temperature decreases gradually from the footprint area into the volume. The temperature in the layer is shown in Fig. 4(*b*) and the temperature difference (ΔT) between the

[1] *Online Materials Information Resource*: http://www.matweb.com/; *Boron Carbide (B4C) – Properties and Information about Boron Carbide*: http://www.azom.com/properties.aspx?ArticleID=75; *Nickel – Properties, Fabrication and Applications of Commercially Pure Nickel*: http://www.nickel-alloys.net/commercially_pure_nickel.html.

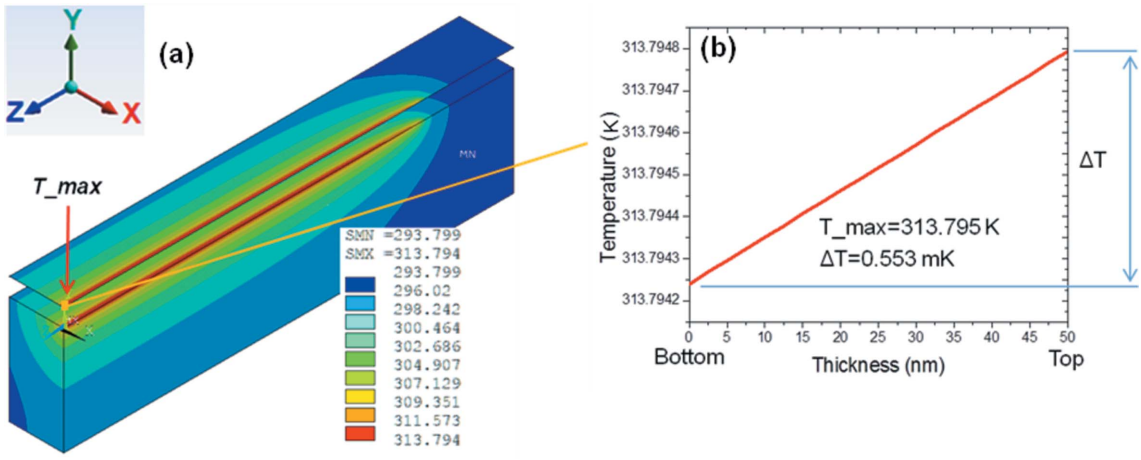

Figure 4
Single-layer mirror, water cooling, thermal results: temperature distribution (*a*) and temperature along the layer thickness (*b*).

Table 1
Bulk material properties of the Si substrate and layer materials (B_4C, Rh, Ni, Pt, Pd).

Online Materials Information Resource: http://www.matweb.com/; *Boron Carbide (B4C) – Properties and Information about Boron Carbide*: http://www.azom.com/properties.aspx?ArticleID=75; *Nickel – Properties, Fabrication and Applications of Commercially Pure Nickel*: http://www.nickel-alloys.net/commercially_pure_nickel.html.

	K (W m^{-1} K^{-1})	α ($\times 10^{-6}$ K^{-1})	E (GPa)	Poisson's ratio ν
Si	148	2.6	112.4	0.28
B_4C	42	6.3	417	0.20
Rh	151	8.5	359	0.26
Ni	60.7	13.1	207	0.31
Pt	69.1	9.1	171	0.39
Pd	71.2	11.1	117	0.39
Cr	69.1	6.2	279	0.21

top and the bottom of the layer is only 0.553 mK. Analytically, by assuming an ideal bottom cooling for the layer part (Fig. 5*a*), the temperature difference can be estimated to be 0.595 mK from equation (1),

$$\Delta T = \frac{P_a \sin(\alpha_{inc})}{k_{B_4C}} t_i = 0.595 \text{ mK}. \quad (1)$$

For the FEA, as the heat flux spread slightly to the side (Fig. 5*b*), ΔT (0.553 mK) is slightly smaller than the estimated value (0.595 mK). The FEA result is in agreement with the analytical estimation.

The deformation result, displacement U_y distribution, is plotted in Fig. 6(*a*). For a comparison, the model with the same geometry and beam condition but not coated is also simulated by FEA. The slope error is defined as the derivative of displacement U_y over position z ($\partial U_y/\partial z$). The slope errors in the footprint area of the two models are compared in Fig. 6(*b*). The difference between the coated and non-coated cases is negligible. The maximum temperature, RMS slope error and peak slope error of the coated and non-coated cases are compared quantitatively in Table 2. The maximum temperature with the coating is higher than without the coating. The CTE of B_4C is higher than that of Si. For the heating process, the coating expands more than the substrate, which will add a convex curvature to the surface and increase the slope error. As the layer is much thinner than the substrate, the values of the maximum temperature and the slope errors are slightly higher for the coated case.

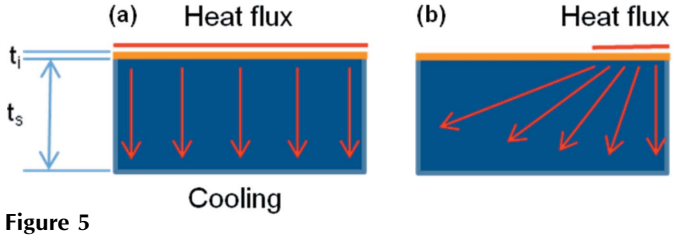

Figure 5
Schematic of the heat flow: ideal case for the analytical estimation (*a*) and FEA (*b*).

The stress results (indicated by the equivalent stress) are shown in Fig. 7. It can be seen (Fig. 7*a*) that the layer stress is much higher (more than ten times) than the stress in the substrate. The maximum stress (S_max) is 48.1 MPa appearing at the center of the top surface and the stress difference (ΔS) between the top and the bottom of the layer is 1645 Pa (Fig. 7*b*). The stress components are listed in Table 3. The normal stress S_y and the three shear stresses (S_{xy}, S_{xz}, S_{yz}) are negligible. The in-plane directional stresses S_x and S_z are the main components. The equivalent stress (S_eqv) is calculated by equation (2) in this case,

$$S\_\text{eqv} \approx \left[\frac{Sx^2 + Sz^2 + (Sx - Sz)^2}{2}\right]^{1/2}. \quad (2)$$

The minus sign indicates that the stress is compressive. As the surface shape is convex, the strain and stress on the top surface of the layer are slightly higher than those on the bottom of the layer. S_z is bigger than S_x because the average temperature along the z direction is bigger than that along the x direction. The maximum equivalent stress of this mirror under water cooling is calculated to be 48.1 MPa, which is much smaller

Table 2
Single-layer mirror, water cooling, results comparison (maximum temperature, RMS slope in footprint area, and peak slope) between coated and non-coated models.

	*T*_max (K)	RMS slope (μrad)	Peak slope (μrad)
Coated	313.795	31.428	70.543
Non-coated	313.794	31.426	70.539

Table 3
Single-layer mirror, water cooling, stress components on the top and bottom of the layer (at the position of Top center) ('–' for compressive).

	X	*Y*	*Z*	*XY*	*XZ*	*YZ*	Eqv
Stress value (MPa) top	−38.491	0	−53.815	0	0	0	48.133
Stress value (MPa) bottom	−38.489	0	−53.813	0	0	0	48.131

than the ultimate tensile strength (UTS) of B_4C (261–569 MPa) (http://www.azom.com/properties.aspx?ArticleID=75). Therefore, the mirror and the coating are working safely.

From Table 2, between the coated and non-coated mirrors, the difference in the maximum temperature is 0.001 K and the difference in the RMS slope is 0.002 μrad. The differences for the temperature and thermal deformation are negligible. However, if the substrate becomes thinner, the influence of the coating on the temperature distribution and thermal deformation will be more significant. It is interesting to know the thickness limit of the substrate from which the influences of the coated layer on the temperature and thermal deformation become no longer negligible. So the simulation is performed for various thicknesses of the silicon substrate in the range 2–60 mm. The results, temperature and RMS slope in half-footprint length *versus* substrate thickness are plotted in Fig. 8. The RMS slope is calculated in half-footprint length to avoid the edge effect of the footprint.

From the simulation, the temperature difference between the coated and non-coated mirrors is negligible even for very thin substrates such as 2 mm (Fig. 8*a*). As shown in Fig. 8(*b*), for the non-coated model (black line), the slope error varies slightly (<2 μrad) when the mirror becomes thinner and tends to a constant of 8.6 μrad. For the coated model, the slope error differs significantly from the non-coated model when the thickness of the substrate is smaller than 10 mm. The RMS slope error of the coated model increases sharply from 9 μrad to above 17 μrad [red line in Fig. 9(*b*)] when the substrate thickness varies from 5 mm to 2 mm. For a 2 mm-thick substrate, the maximum temperature is 492.6 K and the coated

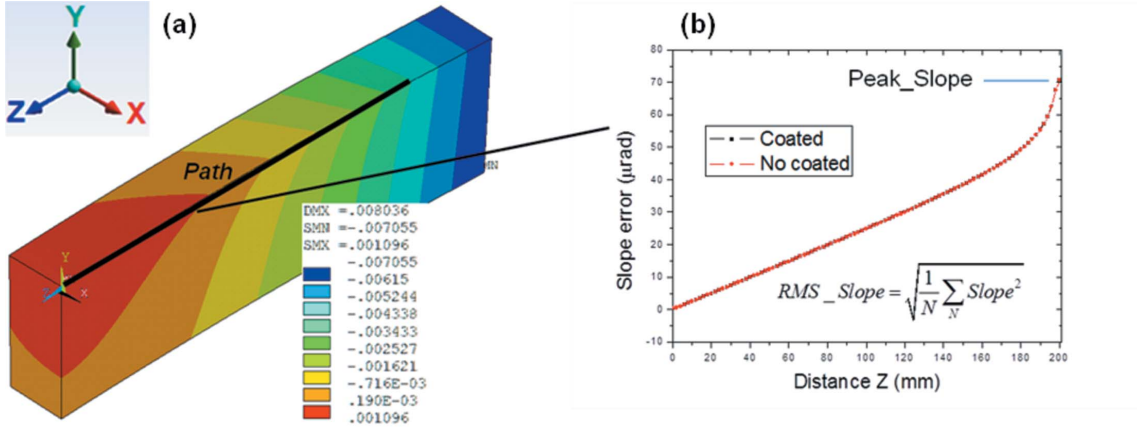

Figure 6
Single-layer mirror, water cooling, deformation results: displacement U_y distribution (*a*) and slope error along the footprint path (*b*).

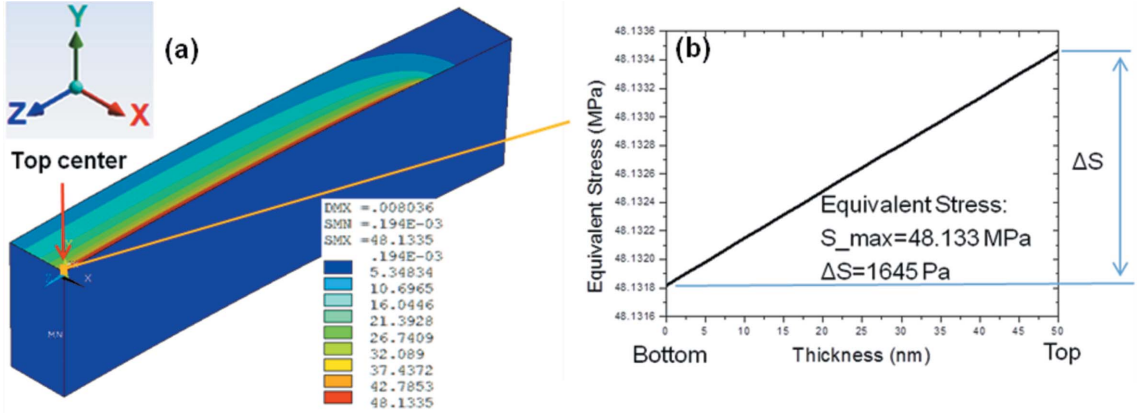

Figure 7
Single-layer mirror, water cooling, stress results: equivalent stress distribution (*a*) and distributed in the layer thickness (*b*).

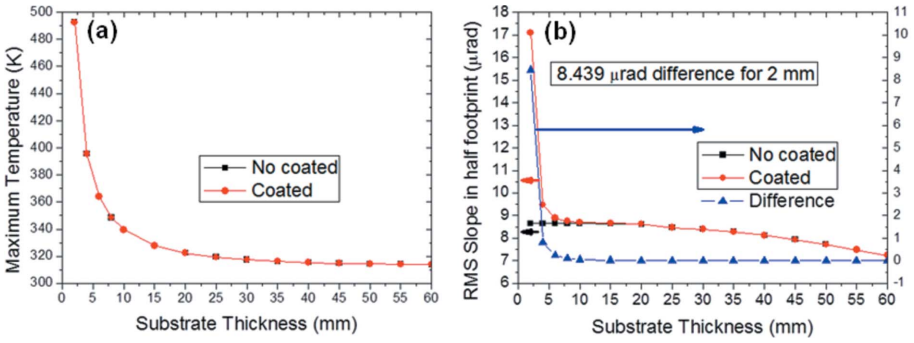

Figure 8
Comparison between coated and non-coated models: maximum temperature (*a*) and RMS slope in half-footprint area (*b*) *versus* substrate thickness.

layer induces an additional thermal slope error of 8.439 μrad RMS compared with the non-coated substrate.

3.1.2. Liquid-nitrogen cooling condition. The liquid-nitrogen cooling condition is applied by setting the cooling temperature to liquid-nitrogen temperature (80 K). The nonlinear thermal conductivity (k) and CTE (α) as shown in Fig. 9 are applied to silicon (Zhang *et al.*, 2013). At cryogenic temperatures, the thermal conductivity of Si (>1.4 W mm^{-1} K^{-1}) is much larger and the CTE of Si ($<-0.4\times10^{-6}$ K^{-1}) is much smaller than those (k = 0.148 W mm^{-1} K^{-1}, $\alpha = 2.6\times10^{-6}$ K^{-1}) at room temperature (293 K). The reference temperature which is defined for the thermal strain calculation is set to be 293 K, which means the layer stress is taken as zero at room temperature. The material properties of B_4C are kept constant as given in Table 1. Geometry and beam conditions are the same as for the water-cooled mirror.

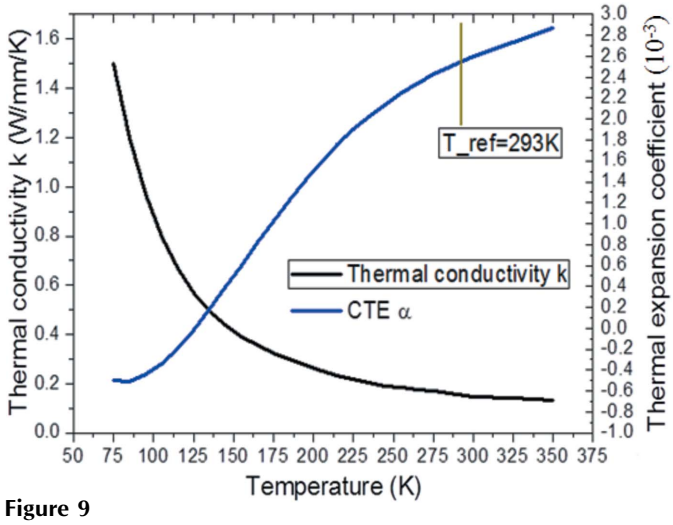

Figure 9
Nonlinear thermal conductivity (k) and CTE (α) of silicon with T_ref = 293 K (Zhang *et al.*, 2013).

As the first step, the temperature is reduced to 80 K uniformly. Theoretically, uniform layer stress will be induced and the surface will be bent spherical. As the CTE of B_4C is larger than the CTE of silicon, for the cooling process, the layer is under tensile stress and the surface shape is concave. The values are estimated to be 575.1 MPa for the layer stress and 0.3×10^{-6} m^{-1} for the curvature from equations (3) (Hsueh, 2002) and (4) (Stoney, 1909), respectively, with $\alpha_{si}\simeq 1.12\times10^{-6}$ K^{-1} at 80 K, where subscripts i and s are for the layer material and the substrate material, respectively,

$$\sigma_i \approx \frac{E_i}{1-\nu_i}(\alpha_s-\alpha_i)\Delta T, \tag{3}$$

$$\Delta\frac{1}{r} \approx \frac{6(1-\nu_s)t_i}{E_s t_s^2}\,\sigma_i. \tag{4}$$

The estimated layer stress from (3) is the value for in-plane stress S_x or S_z. The normal stress S_y and the three shear stresses (S_{xy}, S_{yz}, S_{xz}) are zero and the equivalent stress is calculated by (2), which is equal to S_x or S_z in this situation.

The FEA results are shown in Fig. 10. The layer stress and the surface curvature are 575.0 MPa and 0.3×10^{-6} m^{-1}, respectively, which are in good agreement with the theoretical solution. The stress value of the top surface is slightly lower

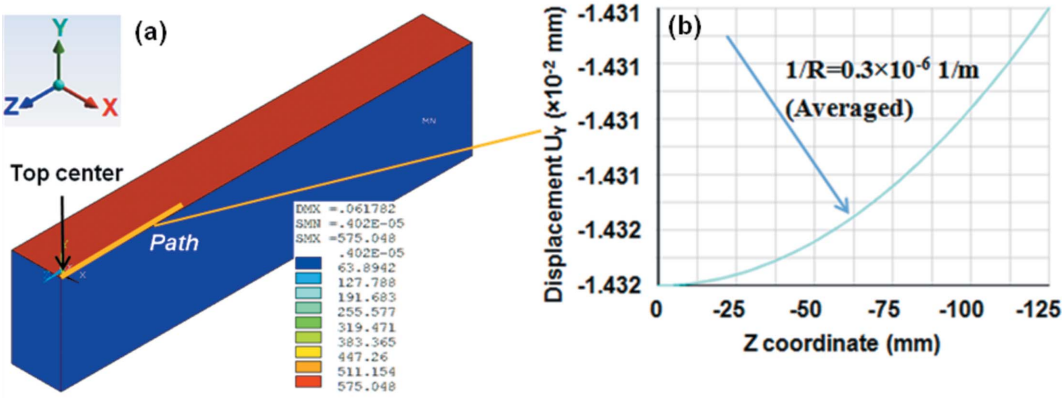

Figure 10
Single-layer mirror, uniformly cooled down from room temperature (293 K) to 80 K, equivalent stress distribution (*a*) and displacement U_y along the path (*b*)

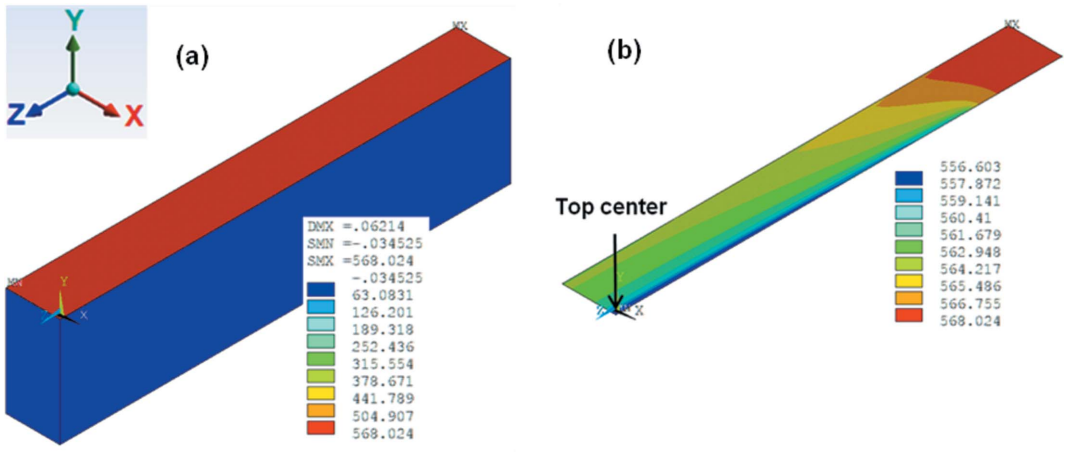

Figure 11
Single-layer mirror, liquid-nitrogen cooling, with heat load: equivalent stress distribution (*a*) and scaled for the layer part (*b*).

than that of the bottom surface for the concave shape. It is opposite to the water-cooled case for which temperature rise and the surface shape is convex.

Secondly, the X-ray beam is illuminated on the top surface. The stress results are shown in Fig. 11. Inside the layer, the stress increases gradually from the footprint area to the side part (Fig. 11*b*). The value varies from 556.6 MPa to 568.0 MPa for S_{eqv}, which is much larger than the stress in the substrate [<63 MPa, all blue in Fig. 13(*a*)]. For the directional stresses, the normal stress S_y and the three shear stresses are zero. The values of S_x and S_z on the top surface are slightly lower (∼0.002 MPa) than the values on the bottom surface for the concave surface shape.

For the liquid-nitrogen cooling condition, as the temperature drops 213 K from room temperature (293 K) to liquid-nitrogen temperature (80 K), large tensile stress of 575.0 MPa is induced inside the layer. When the X-ray beam hits the surface, the optics is heated, which induces a compressive thermal stress in the layer. Combining the tensile stress due to the uniform cooling down to liquid-nitrogen temperature and the X-ray beam-induced compressive stress, the total thermal stress in the layer is reduced slightly to 556.7 MPa, which is 18.3 MPa less than that at 80 K. The heat load of the X-ray beam has slightly released the stress in the coating. Therefore the thermal stress in the footprint area is lower than that in the area far from the footprint. The maximum temperature increase due to the beam heat load is about 5.2 K for this model. The maximum stress appears at the edge of the mirror. From the distribution and variation of the stress, the layer stress at liquid-nitrogen temperature is the most critical issue. In other words, if the layer can survive from the high stress level at liquid-nitrogen temperature, there will be no problem when it is exposed to the X-ray beam. The ultimate tensile strength (UTS) for bulk B_4C at room temperature is 261–569 MPa (http://www.azom.com/properties.aspx?ArticleID=75). The calculated maximum tensile stress (575.0 MPa) is higher than the upper limit of the UTS. Therefore, the coating may NOT survive from the liquid-nitrogen cooling condition. The layer material could be broken by the large tensile stress.

Table 4
Single-layer mirror with different layer materials, summary of layer thermal stress, calculated by bulk material properties.

Coating material	Water cooling	Liquid-nitrogen cooling	UTS
B_4C	48 MPa	575.0 MPa	261–569 MPa
Rh	66 MPa	762.6 MPa	951 MPa
Ni	69 MPa	765.5 MPa	380–620 MPa
Pt	43 MPa	476.5 MPa	120–140 MPa

The strength of a material is defined as its ability to withstand an applied load without failure. The ultimate compressive strength (UCS) and the ultimate tensile strength (UTS) are the limit states of compressive stress and tensile stress, respectively. UCS for a material is generally higher than its UTS. However, the UCS is not often quantified as the failure mode of a material under compressive stress cannot be clearly described. The UTS is used as the stress limit here. Hardening, breakage, necking or sudden breaking may happen for a tensile stress larger than its UTS. For the composite structure with a single layer or multilayer coated on the substrate, another mode of failure resulting from too large stress is the layer delamination, which is the interface effect between the coating and the substrate.

Additionally, some other common-used layer materials are simulated by FEA with the same geometry and beam condition. The material properties and the FEA results are listed in Tables 1 and 4, respectively. As shown in Table 4, the stress levels of all the layers (<100 MPa) are much less than the corresponding UTS for the water-cooling condition. However, only the Rh layer will survive for the liquid-nitrogen cooling. The B_4C, Ni and Pt layer could be damaged by the large tensile stresses under liquid-nitrogen temperature.

3.2. Multilayer white-beam monochromator

Comparing with the single-layer mirror, the multilayer monochromator works with the Bragg reflection for selecting photon energy (Morawe & Osterhoff, 2010). It gives the

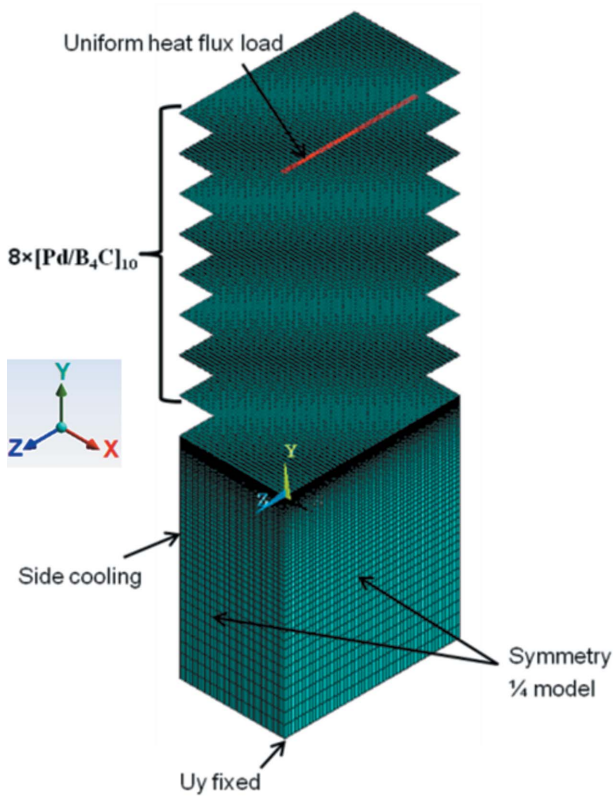

Figure 12
Multilayer monochromator, FE model (for thermal analysis) and boundary conditions.

advantage of a larger grazing angle than the total reflection angle of a mirror, which leads to a shorter footprint and higher power density on the optical surface. The FE model of a multilayer monochromator with typical parameters is shown in Fig. 12. Eighty periods of Pd/B_4C with period thickness 2 nm are coated on a silicon substrate with a geometry of 60 mm × 60 mm × 100 mm. The thicknesses of the sub-layers are equal to each other. The bottom sub-layer is B_4C. The power density is taken as $P_a = 200$ W mm^{-2}. The grazing angle is assumed to be $\alpha_{inc} = 1.5^\circ$ (26.2 mrad). The upstream slits size is 2 mm × 2 mm (H × V), which corresponds to a footprint length of $2/\sin(\alpha_{inc}) = 76.4$ mm.

3.2.1. Water-cooling condition. The convection coefficient and cooling temperature are $h_{cv} = 0.005$ W mm^{-2} K^{-1} and $T_{cool} = 293$ K, respectively, for the water-cooling condition. Results in temperature distribution and temperature along the layer thickness are plotted in Fig. 13. The maximum temperature is 411.0 K and the temperature difference between the top and the bottom of the multilayer part is 14.7 mK. A close-up of the temperature distribution in the top four sub-layers is shown in Fig. 13(*c*). The top sub-layer is Pd. The temperature slope is inversely proportional to the thermal conductivity of each sub-layer material.

The stress results are plotted in Fig. 14. The maximum equivalent stresses are 207.8 MPa and 278.4 MPa for Pd and B_4C sub-layers, respectively, which are much larger than the stress in the substrate [<30 MPa, shown as all blue in Fig. 14(*a*)]. For the stress components, the normal stress S_y and the three shear stresses (S_{xy}, S_{xz}, S_{yz}) are zero. The compres-

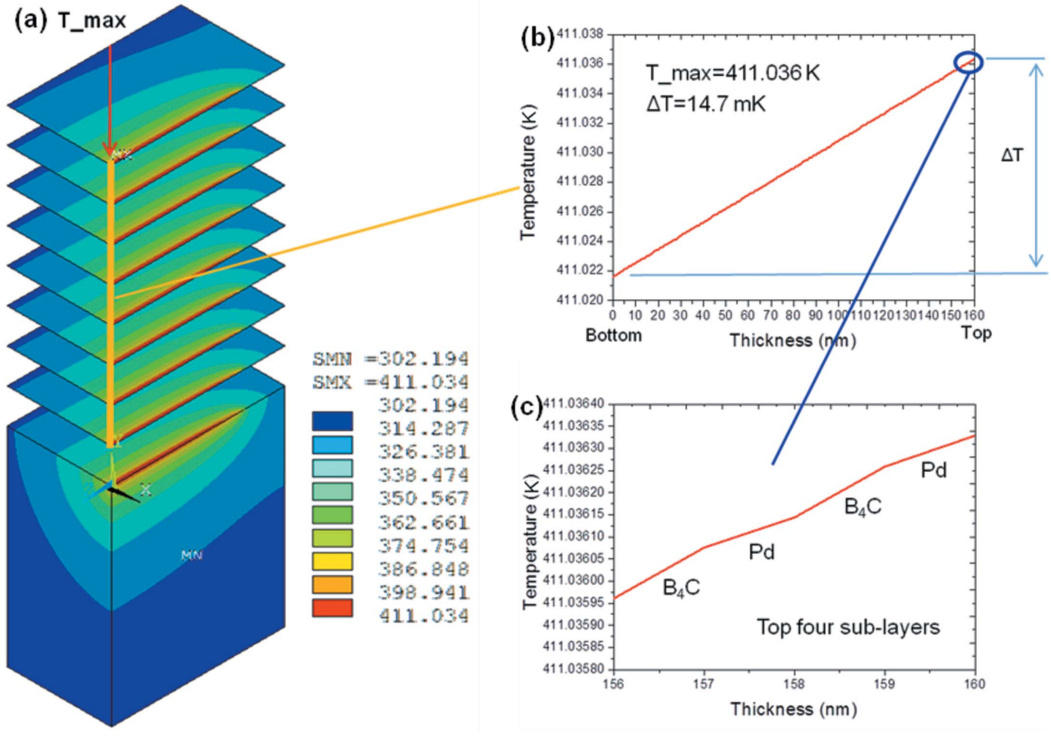

Figure 13
Multilayer, water cooling, thermal results: temperature distribution (*a*), temperature along the layer thickness (*b*) and zoomed for the top four sub-layers (*c*).

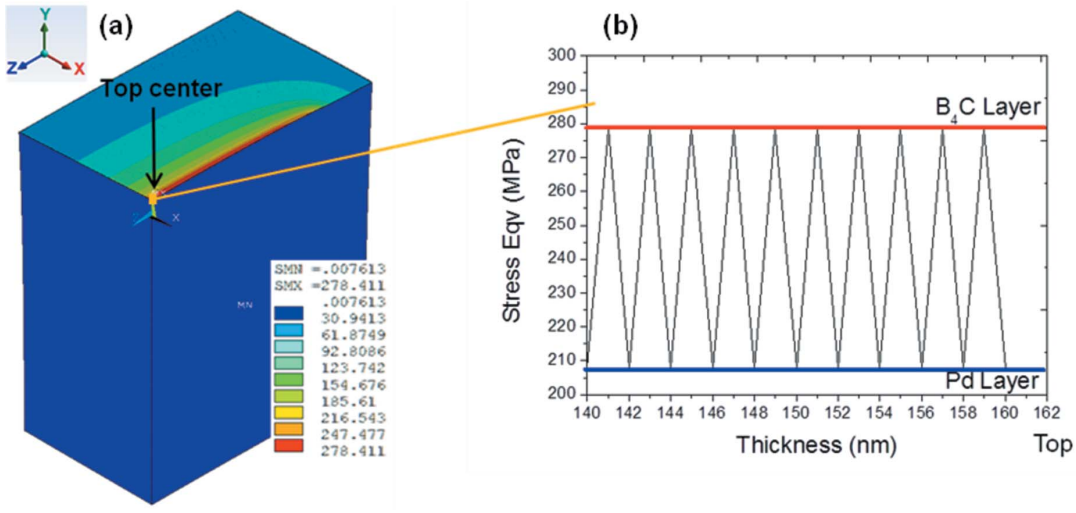

Figure 14
Multilayer, water cooling, stress results: equivalent stress distribution (*a*) and the stresses (*S*_eqv) along layers.

sive in-plane directional stresses S_x and S_z are the main components and the equivalent stress is calculated by equation (2) in such a case. As higher power density and smaller geometry are applied, the stress values are larger than that of the water-cooled single-layer mirror. S_z is larger than S_x because the average temperature along the z direction is larger than that along the x direction. The calculated maximum stress of the B_4C layer (278.4 MPa) is close to the UTS of bulk B_4C (261–569 MPa), as well as that of the Pd layer (208 MPa) being also close to the UTS of bulk Pd (130–320 MPa).

3.2.2. Liquid-nitrogen cooling condition. The liquid-nitrogen cooling condition is applied by setting the cooling temperature to 80 K. The nonlinear thermal conductivity and CTE of silicon (Fig. 9) are applied. The reference temperature is 293 K. The material properties of B_4C and Pd are kept constant (as in Table 1).

The temperature is reduced to 80 K uniformly as the first step. Uniform layer stresses are induced and the surface is bent spherically. As the CTEs of both B_4C and Pd are larger than the CTE of silicon, for the cooling process, tensile layer stresses are formed and the surface shape is concave. Analytically, the stress values are estimated to be 407.7 MPa and 575.1 MPa for the Pd sub-layer and B_4C sub-layer, respectively, from equation (3) with $\alpha_{si} \simeq 1.12 \times 10^{-6}$ K^{-1} at 80 K. The FEA result of the stress in the Pd sub-layer is shown in Fig. 15. The stress values are 407.7 MPa and 575.0 MPa for the Pd sub-layer and B_4C sub-layer, respectively, from FEA, which is in good agreement with the analytical estimation. From equation (3), the thermal stress in the coating sub-layer is proportional to the Young's modulus of the sub-layer material, the difference in CTE between the sub-layer and the substrate, and the temperature change. It is independent of the difference in material properties between different sub-layers. The stress in one sub-layer is independent of the existence of the other sub-layers. In other words, as the sub-layers are very thin compared with the thickness of the substrate, the influence of one sub-layer to another is negligible.

Secondly, the X-ray beam is illuminated on the top surface. As shown in Fig. 15, the sub-layers are under tensile stresses with minimum values of 338.1 MPa and 465.4 MPa for Pd and B_4C sub-layers, which have released 69.6 MPa and 109.6 MPa from the stresses at liquid-nitrogen temperature, respectively. The UTS of bulk B_4C and Pd at room temperature are 261–569 MPa and 130–320 MPa, respectively. Therefore, both sub-layers could be damaged by the large thermal stress under liquid-nitrogen cooling. The re-calculation of layer stresses based on thin-film material properties follows.

3.3. Re-calculation by thin-film material properties

The calculations presented in the previous sections are based on bulk material properties. The thin-film material properties, such as Young's modulus and CTE, can be very different from their bulk statuses. These thin-film material properties depend not only on the film thickness but also on the fabrication technique. Very little data on film materials can be found in the literature. We have carried out experiments to measure the thin-film material properties of the layer coating for multilayer optics. Refer to Cheng *et al.* (2014) for more details of the experiment. Here we use the experimental results to re-calculate the thermal stresses.

As shown in Fig. 16, the Young's moduli of thin films are significantly smaller than those of bulk materials. The Young's moduli of 50 nm B_4C, Pd and Cr layers have been measured to be 41.8 ± 31.4 GPa, 53.8 ± 9.5 GPa and 113 ± 34.3 GPa, respectively. Compared with the bulk materials, the Young's modulus of these thin films are reduced by a factor of ten for B_4C layer and by a factor of more than two for the Pd and Cr layers. We take a factor of ten for the B_4C layer and a factor of two for the Pd and Cr layers for the re-calculation. Extrapolating that for Rh, Ni and Pt layers, the Young's moduli are also reduced by a factor of two, which is consistent with Pd and Cr thin-film layers. The thermal stresses of the layers are reduced correspondingly.

Table 5
Single-layer mirror with different layer materials, layer stresses recalculated by thin-film material properties.

	Water cooling	Liquid-nitrogen cooling	UTS
Pt	10.8 MPa	238.3 MPa	> −120–140 MPa
B_4C	4.8 MPa	57.5 MPa	> −261–569 MPa
Rh	16.5 MPa	381.3 MPa	> −951 MPa
Ni	17.3 MPa	382.8 MPa	> −380–620 MPa

The recalculated results of a single-layer mirror by thin-film material properties are shown in Table 5. For the water-cooling condition, the layer stresses are much smaller than their UTS. This indicates that all the layers will be safe from thermal stresses. For the liquid-nitrogen cooling condition, coatings of B_4C, Rh and Ni will work well. For the Pt layer, however, the layer stress is higher than the UTS of Pt. However, the UTS here are for the bulk materials at room temperature. Empirically, the UTS of thin films are larger than these values. There are still some uncertainties about whether the Pt-coated mirror will be damaged by the layer stress under liquid-nitrogen cooling.

A summary of the layer thermal stresses in the multilayer monochromator is given in Table 6. The thin-film material properties are applied by reducing the Young's modulus by a factor of ten for the B_4C layer and by a factor of two for the Pd layer. The recalculated stresses of the multilayer monochromator by thin-film material properties are summarized in Table 7. This shows that the Pd sub-layer in the multilayer monochomator may not survive from the stresses at liquid-nitrogen temperature.

Furthermore, in most thin-film coatings, considerable compressive intrinsic stress exists caused by the deposition

Table 6
Multilayer, stress summary calculated by bulk material properties.

	Water cooling	Liquid-nitrogen cooling	UTS
B_4C sub-layer	278 MPa	575 MPa	261–569 MPa
Pd sub-layer	208 MPa	408 MPa	130–320 MPa

Table 7
Multilayer, stresses re-calculated by thin-film material properties.

	Water cooling	Liquid-nitrogen cooling	UTS
B_4C sub-layer	27.8 MPa	57.5 MPa	>261–569 MPa
Pd sub-layer	104 MPa	204 MPa	>130–320 MPa

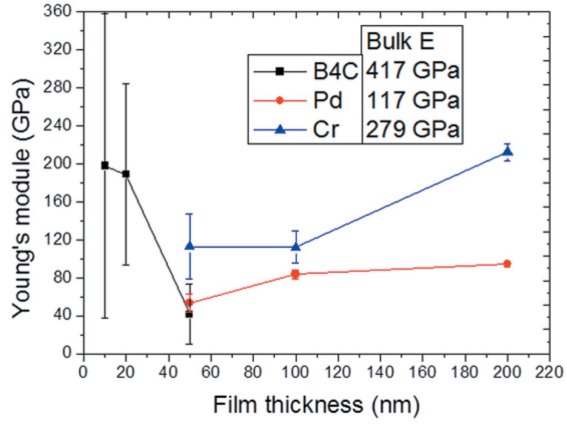

Figure 16
Experimental results, Young's modulus of thin films: B_4C of 10 nm, 20 nm, 50 nm; Pd of 50 nm, 100 nm, 200 nm; Cr of 50 nm, 100 nm, 200 nm.

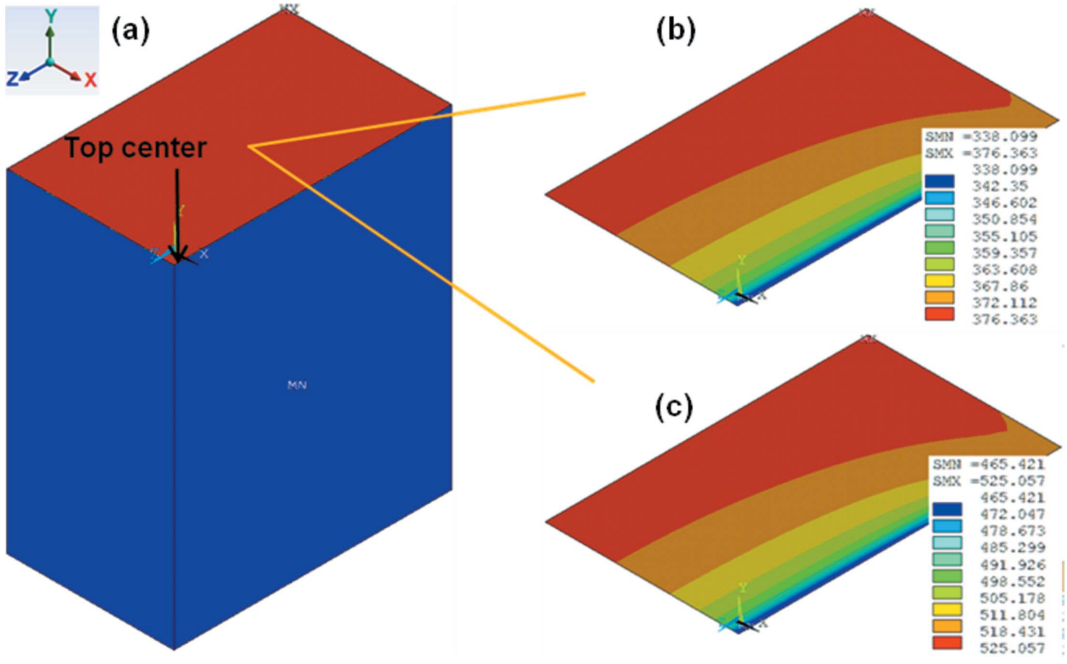

Figure 15
Multilayer, liquid-nitrogen cooling, with heat load, equivalent stress distribution: the whole model (*a*), in Pd sub-layer (*b*) and in B_4C sub-layer (*c*).

process. For example, more than 1 GPa of compressive intrinsic stress has been observed for a B_4C layer of thickness 5–25 nm at room temperature (Morawe *et al.*, 2010). The stress results from FEA will represent the changes in stress with the intrinsic stress as an initial state. For the liquid-nitrogen cooling, when the optics is cooled down, the compressive intrinsic stress is released. As a result, the layer is under smaller tensile stress than the above calculation, or even under compressive stress at the liquid-nitrogen temperature depending on the value of the intrinsic stress. This intrinsic stress can counterbalance partially the tensile stress in the coating layer when the optics is cooled down from room temperature to liquid-nitrogen temperature.

4. Conclusion

Potential damage due to the heat load from the intense synchrotron radiation white beam is a critical issue for the design of multilayer-based white-beam optics. The influence of the coatings on temperature and deformation are negligible. However, very large layer stress is induced from the thermal mismatch (different thermal expansion coefficients) between the layer and the substrate materials. The stress in the substrate is only slightly increased (<0.1%).

For the water-cooling condition, the layer is under compressive stress of tens of MPa induced by the X-ray beam power. The compressive thermal stress is normally much less than the strength (UTS) of the layer material. For the liquid-nitrogen cooling condition, however, a large tensile stress of several hundreds of MPa is formed in the layer as the optics is cooled down to liquid-nitrogen temperature. This tensile thermal stress can exceed the UTS of the layer for some kinds of materials. The FEA results show that the Pt layer for the mirror and the Pd sub-layer in the multilayer monochomator may not survive from the stresses at liquid-nitrogen temperature. The compressive intrinsic stress from the deposition process is a positive factor for the tensile thermal stress issue.

The thermal stress in multilayer optics depends on the difference in CTE between the layer material and the substrate material, but it is independent of the CTE difference between different sub-layers. In principle, to minimize the thermal stress, the coating material should have a CTE closer to that of the substrate, and/or a smaller Young's modulus.

The authors would like to thank Dr Raymond Barrett for fruitful discussions. They also thank Professor Dr Olivier Thomas and Dr Ray Conley for their co-reviewing of this work.

References

Cheng, X., Morawe, C., Peffen, J.-Ch. & Zhang, L. (2014). *Proc. SPIE*, **9207**, 920709.
Friedrich, K., Morawe, C., Peffen, J.-Ch. & Osterhoff, M. (2011). *Proc. SPIE*, **8077**, 80770M.
Hsueh, C. H. (2002). *Thin Solid Films*, **418**, 182–188.
Morawe, C. & Osterhoff, M. (2010). *X-ray Opt. Instrum.* **2010**, 479631.
Morawe, C., Peffen, J.-Ch & Friedrich, K. (2010). *Proc. SPIE*, **7208**, 78020B.
Stoney, G. G. (1909). *Proc. R. Soc. London Ser. A*, **82**, 172.
Zhang, L., Sánchez del Río, M., Monaco, G., Detlefs, C., Roth, T., Chumakov, A. I. & Glatzel, P. (2013). *J. Synchrotron Rad.* **20**, 567–580.